tvst

Retina

Characterization of Ocular Morphology in Col4a3$^{-/-}$ Mice as a Murine Model for Alport Syndrome

Yuwei Wang[1,*], Ruilin Zhu[1,*], Liang Zhao[1], Fang Wang[2], Yanqin Zhang[2], Shiguang Liu[3], Jie Ding[2], and Liu Yang[1]

[1] Department of Ophthalmology, Peking University First Hospital, Xicheng District, Beijing, China
[2] Department of Pediatrics, Peking University First Hospital, Xicheng District, Beijing, China
[3] Sanofi Clinical Development, Cambridge, MA, USA

Correspondence: Liu Yang, Department of Ophthalmology, Peking University First Hospital, No. 8 Xi Shi Ku Street, Xicheng District, Beijing 100034, China. e-mail: liu_yang@bjmu.edu.cn

Received: November 9, 2023
Accepted: May 27, 2024
Published: July 23, 2024

Keywords: alport syndrome (AS); collagen IV; basement membrane; müller cell; animal model

Citation: Wang Y, Zhu R, Zhao L, Wang F, Zhang Y, Liu S, Ding J, Yang L. Characterization of ocular morphology in Col4a3$^{-/-}$ mice as a murine model for alport syndrome. Transl Vis Sci Technol. 2024;13(7):16, https://doi.org/10.1167/tvst.13.7.16

Purpose: The purpose of this study was to investigate the ocular morphological characteristics of Col4a3$^{-/-}$ mice as a model of Alport syndrome (AS) and the potential pathogenesis.

Methods: The expression of collagen IV at 8, 12, and 21 weeks of age was evaluated by immunohistochemistry in wild-type (WT) and Col4a3$^{-/-}$ mice. Hematoxylin and eosin (H&E) staining and thickness measurements were performed to assess the thickness of anterior lens capsule and retina. Ultrastructure analysis of corneal epithelial basement membrane, anterior lens capsule, internal limiting membrane (ILM), and retinal pigment epithelium (RPE) basement membrane was performed using transmission electron microscopy. Finally, Müller cell activation was evaluated by glial fibrillary acidic protein (GFAP) expression.

Results: Collagen IV was downregulated in the corneal epithelial basement membrane and ILM of Col4a3$^{-/-}$ mice. The hemidesmosomes of Col4a3$^{-/-}$ mice corneal epithelium became flat and less electron-dense than those of the WT group. Compared with those of the WT mice, the anterior lens capsules of Col4a3$^{-/-}$ mice were thinner. Abnormal structure was detected at the ILM Col4a3$^{-/-}$ mice, and the basal folds of the RPE basement membrane in Col4a3$^{-/-}$ mice were thicker and shorter. The retinas of Col4a3$^{-/-}$ mice were thinner than those of WT mice, especially within 1000 µm away from the optic nerve. GFAP expression enhanced in each age group of Col4a3$^{-/-}$ mice.

Conclusions: Our results suggested that Col4a3$^{-/-}$ mice exhibit ocular anomalies similar to patients with AS. Additionally, Müller cells may be involved in AS retinal anomalies.

Translational Relevance: This animal model could provide an opportunity to understand the underlying mechanisms of AS ocular disorders and to investigate potential new treatments.

Introduction

Alport syndrome (AS) is an inherited disease characterized by progressive renal failure, hearing loss, and ocular abnormalities. This disease is caused by mutations in the collagen IV genes COL4A3, COL4A4, and COL4A5, which lead to deficiency of the type IV $\alpha3\alpha4\alpha5$ collagen network in the basement membrane.[1–3] The common ocular features of AS include corneal clouding, anterior lenticonus, fleck retinopathy, and temporal retinal thinning.[1,4,5] In recent years, ocular manifestations of AS have been increasingly reported.[6–8] However, it is difficult to obtain ocular tissue from patients, especially retina and cornea samples; thus, associated research on AS tissue is limited. Studies on ocular changes in patients with AS have focused mainly on clinical manifestations, and few of them have used histologic or molecular research. An animal model with phenotypic recapitulation of

AS-associated ocular features is useful to study pathogenesis of this disease.

Col4a3$^{-/-}$ mice is widely used as a murine model for autosomal AS. The Col4a3$^{-/-}$ mouse model develops progressive glomerulonephritis with microhematuria and proteinuria, recapitulating the main features of human AS.[9,10] No previous reports have described the ocular characteristics of Col4a3$^{-/-}$ mice, and the effects of Col4a3 gene knockout on the eyes have not been characterized. Whether this model is suitable for investigating ocular abnormalities in patients with AS is unknown. We performed this study to characterize the effects of the Col4a3 knockout mutation on the visual system. The goal of the analyses was to determine whether Col4a3$^{-/-}$ mice are a suitable model for assessing ocular abnormalities in patients with AS and to explore the potential pathogenesis of these changes.

Materials and Methods

Animals

All animal experiments were performed in accordance with the guidelines of the Association for Research in Vision and Ophthalmology (ARVO) Statement for the Use of Animals in Ophthalmic and Vision Research and in accordance with the Animal Care Committee of Peking University First Hospital.

The Col4a3 knockout mice on 129 × 1/SvJ background, 129-Col4a3^{tm1Dec}/J, were obtained from the Jackson Laboratory (JAX stock #002908). We generated Col4a3 knockout mice on the C57BL/6J background (Col4a3$^{-/-}$) by backcrossing the 129-Col4a3^{tm1Dec}/J to the C57BL/6J background for more than 10 generations, as previously described.[10] At 8, 12, and 21 weeks of age, Col4a3$^{-/-}$ mice and their wild type (WT) littermates were euthanized. The eyeballs were enucleated and fixed immediately for light and electron microscopy. This study used 2 female mice and 2 male mice at the age of 8 weeks, 2 females and 1 male at the age of 12 weeks, and 3 females and 1 male at the age of 21 weeks.

DNA was isolated from tail biopsies with EasyPure Genomic DNA Kit (TransGen Biotech, Beijing, China). Genotyping was performed using the separated polymerase chain reaction (PCR) protocol provided by the Jackson Laboratory. The primer sequences are listed in the Supplementary Table S1. In addition, to validate the knockout efficiency of Col4a3 in our Col4a3$^{-/-}$ model, we performed quantitative real-time PCR (Supplementary Methods and Materials; Supplementary Table S2) for Col4a3 mRNA expression.

Hematoxylin-Eosin Staining

The enucleated eyeballs were fixed in 4% paraformaldehyde (PFA) at room temperature overnight, embedded in paraffin, and then sectioned at a thickness of 4 µm through the optic nerve head. The sections were stained with hematoxylin for 4 minutes and eosin for 3 minutes, dehydrated with ethanol and xylene, and then sealed with neutral glue. Then, the sections were examined with a light microscope (Nikon, Japan).

Thickness Measurements of Retina and Anterior Lens Capsule

CaseViewer software (version 2.4, 3DHistech, Hungary) was used to evaluate morphometric changes. The thickness of the retina (measured from the inner edge of the retinal pigment epithelium to the internal limiting membrane) was measured at nine equidistant positions (200 µm intervals) between the optic nerve head (ONH) and periphery of the retina. The ganglion cell layer (GCL), inner plexiform layer (IPL), inner nuclear layer (INL), and outer nuclear layer (ONL) thicknesses were measured at a distance of 1 mm to the ONH as previously described.[11]

The thickness of the anterior lens capsule was measured at 3 points, including the center of the pupil and 100 µm away from the pupil center on both the nasal and temporal sides. The average thickness of the three points was calculated for each eye.

Four mice in each age group of both Col4a3$^{-/-}$ mice and WT mice were measured. The retinal and anterior lens capsule thicknesses were analyzed statistically.

Immunohistochemistry

After dewaxing and rehydration, 4-µm-thick sections were soaked in Tris/EDTA buffer (pH 9.0) for heat-induced antigen retrieval. Endogenous peroxidase activity was quenched by incubation with peroxidase block (Rabbit Two-Step Process Kit, PV-6001; ZSGB-Bio, Beijing, China) for 30 minutes at room temperature. Following incubation with 10% goat serum for 1 hour at room temperature to block the nonspecific binding sites, the sections were incubated with anti-collagen IV antibody (1:1000, ab236640; Abcam) or anti-GFAP antibody (1:800, ab207165; Abcam) overnight at 4°C. As a negative control, the primary antibody was omitted. Subsequently, enzyme-

conjugated goat anti-rabbit IgG antibodies (Rabbit two-step process kit, PV-6001; ZSGB-Bio, Beijing, China) were added for 2 hours at room temperature. Finally, the sections were visualized with DAB (1:20, ZLI-9018; ZSGB-Bio, Beijing, China) and counterstained with hematoxylin. The positive signals representing collagen IV and GFAP expression (brown color) were examined by optical microscopy (Nikon, Japan).

Transmission Electron Microscopy

Mouse eyeballs collected for transmission electron microscopy (TEM) analysis were fixed in 3% glutaraldehyde immediately after enucleation, gently dissected into corneas, lenses, and eye cups, and then kept at 4°C overnight. After washing with phosphate-buffered saline (PBS), the samples were fixed in 1% osmium tetroxide (OsO4) for 2 hours and then dehydrated in a graded dilution of absolute ethanol. After that, the specimens were embedded in Epon, sectioned into 70 to 90 nm thick ultrathin sections, and stained with 5% uranyl acetate and lead citrate. The sections were observed and photographed under a TEM (JEM-1400Flash; JEOL, Tokyo, Japan).

Statistical Analysis

The quantitative results are presented as the mean ± SD. The statistical significance of the differences in retinal morphology was analyzed using 2-way analysis of variance (ANOVA) with multiple comparisons. Unpaired Student's *t*-tests were performed for comparisons of collagen IV expression, GFAP expression, lens capsule thickness, GCL thickness, IPL thickness, INL thickness, ONL thickness, and Col4a3 mRNA expression between the two groups. Statistical significance was set at $P < 0.05$. All the statistical analyses were performed using GraphPad Prism 9 (GraphPad Software, San Diego, CA, USA).

Results

In this study, we examined the Col4a3 mRNA expression and confirmed the Col4a3 was knocked out in corneas, lenses, and retinas of Col4a3$^{-/-}$ mice (Supplementary Fig. S1). We examined abnormal corneal, lens and retinal structures in Col4a3$^{-/-}$ mice by hematoxylin and eosin (H&E) staining, thickness measurements, immunohistochemistry, and TEM to explore the mechanisms involved in AS ocular manifestations.

Abnormal Structure of the Corneal Epithelial Basement Membrane in Col4a3$^{-/-}$ Mice

Collagen IV immunohistochemical staining was performed to observe the protein expression in the cornea. In WT mice, collagen IV was found to be expressed in both the corneal epithelial basement membrane (Fig. 1A, red arrows) and the corneal endothelial basement membrane (Descemet's membrane; Fig. 1B, blue arrows). In Col4a3$^{-/-}$ mice, the expression of collagen IV in the corneal epithelial basement membrane was decreased and the corneal epithelial basement membrane appeared discontinuity in all age groups (Fig. 1C). No significant abnormalities in collagen IV expression in the corneal endothelial basement membrane were detected in the Col4a3$^{-/-}$ mice (Fig. 1D).

To observe the ultrastructural changes in the corneal epithelial basement membrane in Col4a3$^{-/-}$ mice, we conducted TEM analysis. In the WT group, hemidesmosomes composed of electrically dense plaques tightly adhered to the corneal epithelial basement membrane and presented a triangular shape (Fig. 1E, left panel, yellow arrowheads). However, in the Col4a3$^{-/-}$ group, the hemidesmosomes in some regions became flat and less electron-dense than those in the WT group and seemed to be sparsely distributed or even absent in some regions (see Fig. 1E, right panel, yellow arrowheads). These findings may indicate that the connection between corneal epithelial cells and the basement membrane was weak in Col4a3$^{-/-}$ mice and that epithelial cells were more prone to detachment.[12,13]

Anterior Lens Capsule Thinning and Lens Morphological Anomalies in Col4a3$^{-/-}$ Mice

Collagen IV is widely expressed in the anterior lens capsule of mice.[14,15] Using immunohistochemical staining, collagen IV was detected in WT mice (Fig. 2A, black asterisks) and Col4a3$^{-/-}$ mice (see Fig. 2A, white asterisks). However, there was no obvious difference in collagen IV expression between Col4a3$^{-/-}$ mice and WT mice in either age group (Fig. 2C).

The thicknesses of the anterior lens capsules of Col4a3$^{-/-}$ mice and age-matched WT mice were measured (Figs. 2B, 2D). No significant difference between the Col4a3$^{-/-}$ mice and WT mice was found in the 8-week-old group (see the Table, $P = 0.1027$; Fig. 2D). In contrast, the anterior capsule of the Col4a3$^{-/-}$ mice was significantly thinner than that of the WT mice in the 12-week-old group (see the Table, $P = 0.0020$; Fig. 2D) and in the 21-week-old group (see the Table, $P = 0.0006$; Fig. 2D).

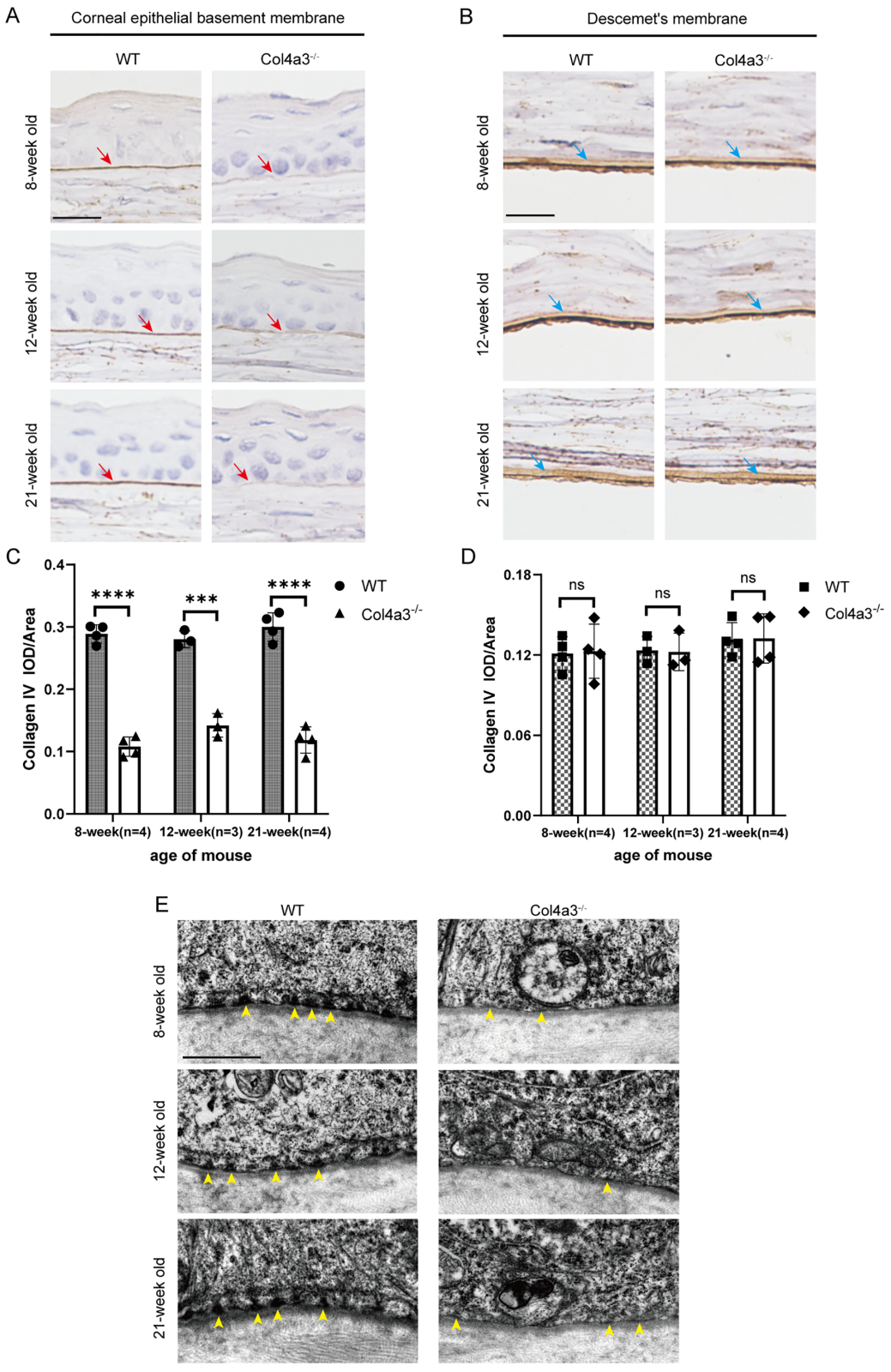

Figure 1. Abnormal corneal epithelial basement membrane structure in Col4a3$^{-/-}$ mice. Collagen IV expression was downregulated in the (**A**) corneal epithelial basement membrane (*red arrows*) of Col4a3$^{-/-}$ mice but not in the (**B**) corneal endothelial basement membrane (*blue arrows*). Bar = 20 µm. Collagen IV expression in the (**C**) corneal epithelial basement membrane and in the (**D**) corneal endothelial basement membrane was quantified via immunohistochemistry images (n = 3–4). Data are shown as mean ± SD (ns = P value > 0.05; *** = P value < 0.001; **** = P value < 0.0001). (**E**) The hemidesmosomes (*yellow arrowheads*) consisted of electron-dense plaques that were equally and tightly adherent to the basal lamina in WT mice (*left panel*), but in Col4a3$^{-/-}$ mice (*right panel*), the hemidesmosomes were flat, and less electron density even disappeared in some regions. Bar = 1 µm.

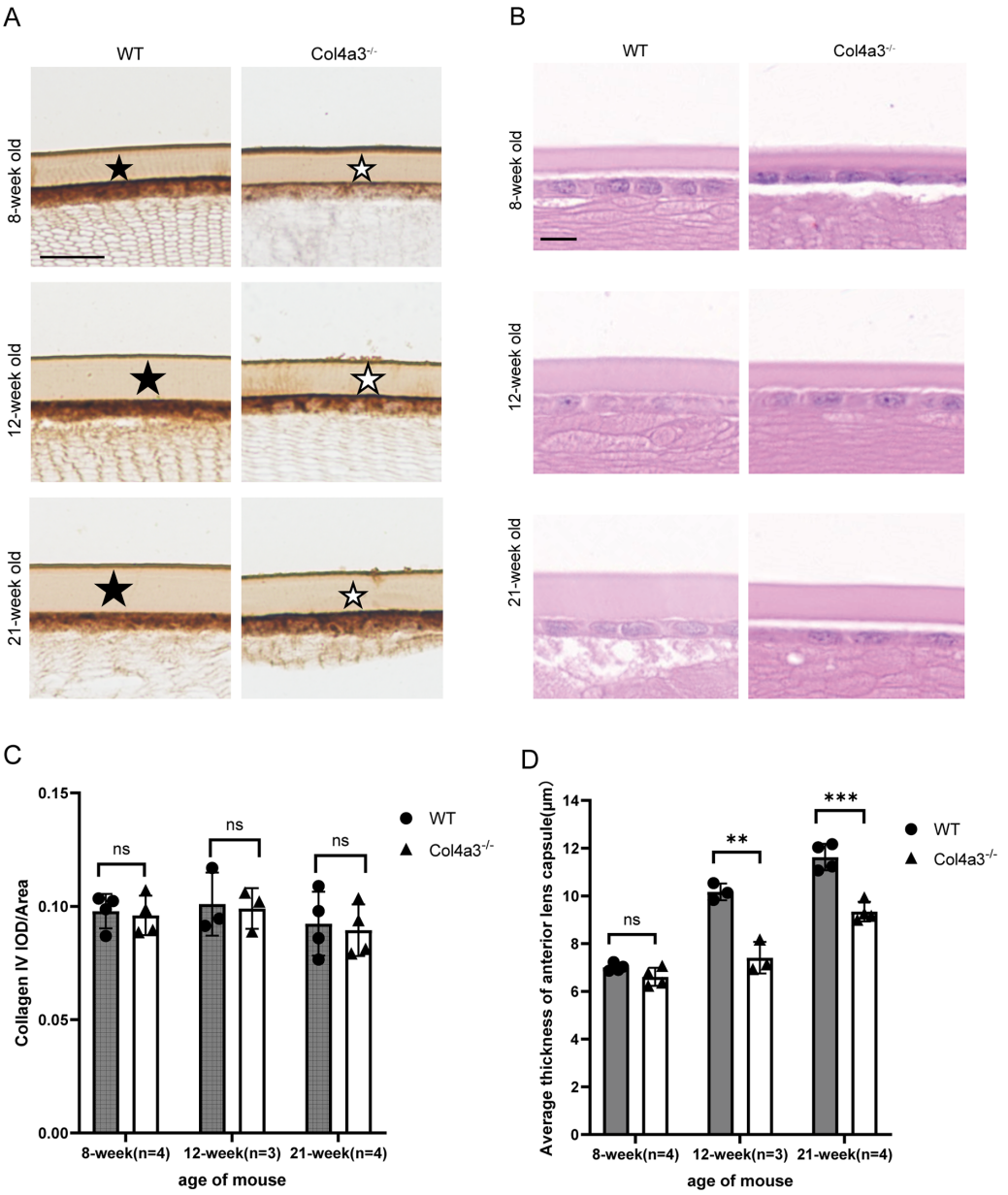

Figure 2. The anterior lens capsules thinner in Col4a3$^{-/-}$ mice. (**A**) Collagen IV expression in the anterior lens capsule was detected in both WT group (*black asterisks*) and the Col4a3$^{-/-}$ group (*white asterisks*). Bar = 20 µm. (**B**) Representative images of H&E staining showing that the anterior lens capsules of Col4a3$^{-/-}$ mice were thinner than those of WT mice. Bar = 10 µm. (**C**) Quantifications of collagen IV expression in the anterior lens capsule were analyzed on immunohistochemistry images (n = 3–4). Data are shown as mean ± SD (ns = P value > 0.05). (**D**) Qualifications of the thicknesses of anterior lens capsule were analyzed via H&E staining images (n = 3–4). Data are shown as mean ± SD (ns = P value > 0.05; ** = P value < 0.01; *** = P value < 0.001).

TEM analysis revealed that the anterior lens capsule exhibited a homogeneous membrane structure and no obvious abnormalities in Col4a3$^{-/-}$ mice (Supplementary Fig. S2). By measuring the thickness of the anterior lens capsule, it was found that the anterior lens capsule in Col4a3$^{-/-}$ mice was thinner than that in WT mice in the 12-week-old and 21-week-old groups (see Supplementary Fig. S2), which was consistent with the H&E staining results (see Figs. 2B, 2D). However, because fewer than three mice in each group were observed by electron microscopy, statistical analysis was not conducted on the thickness of the anterior lens capsule measured by electron microscopy.

Interestingly, we detected an "anterior lenticonus-like" structure in two 21-week-old Col4a3$^{-/-}$ mice, which presented protruding anterior poles of the lens, similar to a "ridge" shape (Fig. 3A, right). TEM analysis revealed that the anterior lens capsule of the most

Table. The Thickness of Anterior Lens Capsules in Col4a3$^{-/-}$ Mice and Age-Matched Wild Type Mice

Age Group	Col4a3$^{-/-}$ (μm)	WT (μm)	*P* Value
8-week-old ($n = 4$)	6.61 ± 0.38	7.01 ± 0.16	0.1027
12-week-old ($n = 3$)	7.41 ± 0.66	10.17 ± 0.35	0.0020
21-week-old ($n = 4$)	9.34 ± 0.41	11.62 ± 0.56	0.0006

Mean ± SD

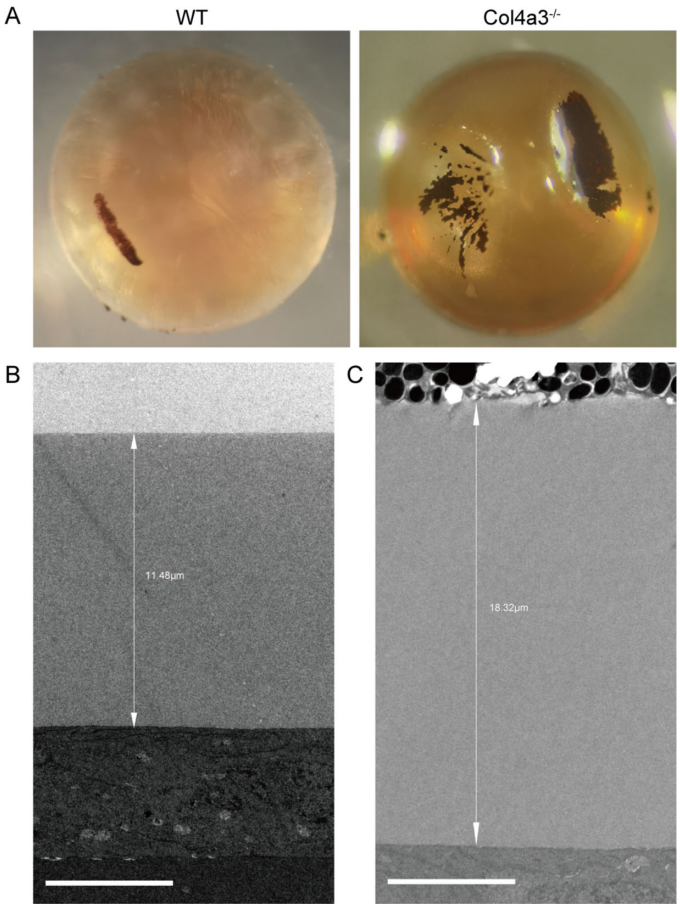

Figure 3. "Anterior lenticonus-like" structure in two 21-week-old Col4a3$^{-/-}$ mice. (**A**) Representative images of the "anterior lenticonus-like" structure observed in 21-week-old Col4a3$^{-/-}$ mice under light a microscope. The anterior lens capsule of (**B**) the most protruding part was thinner than that of (**C**) the adjacent concave part according to TEM. Bar = 5 μm.

protruding part (Fig. 3B) was thinner than the adjacent concave part of the lens in Col4a3$^{-/-}$ mice (Fig. 3C). Nevertheless, we did not observe other abnormalities in the internal structure of the anterior lens capsule.

Changes in Collagen IV Expression in the Retinas of Col4a3$^{-/-}$ Mice

Collagen IV was detected in the retinal internal limiting membrane (ILM) of WT mice via immunohistochemical staining (Fig. 4A, red arrows), whereas in Col4a3$^{-/-}$ mice (see Fig. 4A, green arrows) the expression of collagen IV decreased in each age group (Fig. 4C). TEM analysis revealed that the ILMs of the WT mice in each age group had homogeneous electron density (Fig. 4B, red asterisks). In Col4a3$^{-/-}$ mice, an abnormal membrane-like structure was detected in the inner part of the retina in each age group, the continuity of the ILM was lost, and the ILM collagen fibrils became loose and fragmented (see Fig. 4B, green asterisks).

Collagen IV was also detected in the basement membrane of the retinal pigment epithelium (RPE) of both the WT mice and Col4a3$^{-/-}$ mice (Fig. 5A), and no obvious difference was detected between the two groups according to the immunohistochemical staining images. Due to the similarity in color between the RPE basement membrane and surrounding pigment particles observed in the immunohistochemical image, quantitative analysis of the RPE basement membrane was not feasible. TEM analysis revealed strip-like basal folds in the retinal pigment epithelium basement membrane in WT mice. These folds are closely connected to each other and to the basement membrane, exhibiting slightly hyper electron density at the junction sites (Fig. 5B, yellow asterisks). On the other hand, the basal folds of the RPE basement membrane of Col4a3$^{-/-}$ mice became thicker, shorter, and sparser and even disappeared in some regions (see Fig. 5B, blue asterisks).

Retinal Thickness Reduction in Col4a3$^{-/-}$ Mice

Light microscopy with H&E staining was used to investigate retinal morphological changes in Col4a3$^{-/-}$ mice (Fig. 6A). The measurements of the retinas at a series points indicated that the retinas within 1000 μm away from the ONH were significantly thinner (all $P < 0.05$) in the Col4a3$^{-/-}$ mice than in the WT mice in all age groups (Figs. 6B–6G). The retinal thickness of 8-week-old Col4a3$^{-/-}$ mice at 1200 μm and 1400 μm from the ONH was significantly thinner than that of age-matched WT mice (see Figs. 6E–6G).

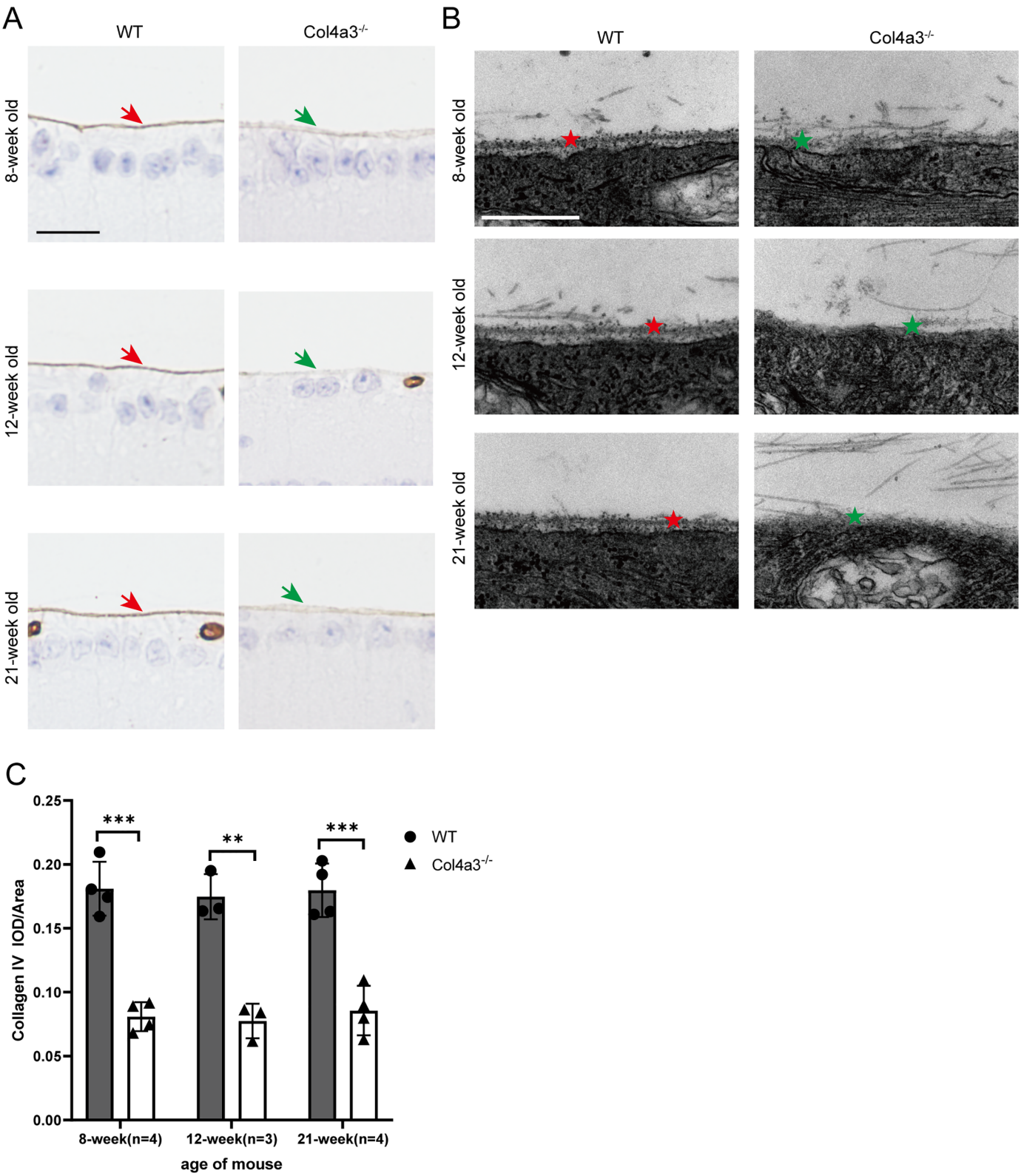

Figure 4. Abnormal membranous structure of the internal limiting membrane (ILM) in Col4a3$^{-/-}$ mice. (**A**) Collagen IV expression in the ILM of Col4a3$^{-/-}$ mice (*red arrows*) was lower than that in the ILM of WT mice (*green arrows*). Bar = 20 µm. (**B**) TEM revealed better continuity and more homogeneous electron density in the ILM of WT mice (*red asterisks*) but abnormal membrane-like structures in Col4a3$^{-/-}$ mice (*green asterisks*). Bar = 500 nm. (**C**) Quantifications of collagen IV expression in ILM were analyzed on immunohistochemistry images ($n = 3$–4). Data are shown as mean ± SD. ** = P value < 0.01; *** = P value < 0.001.

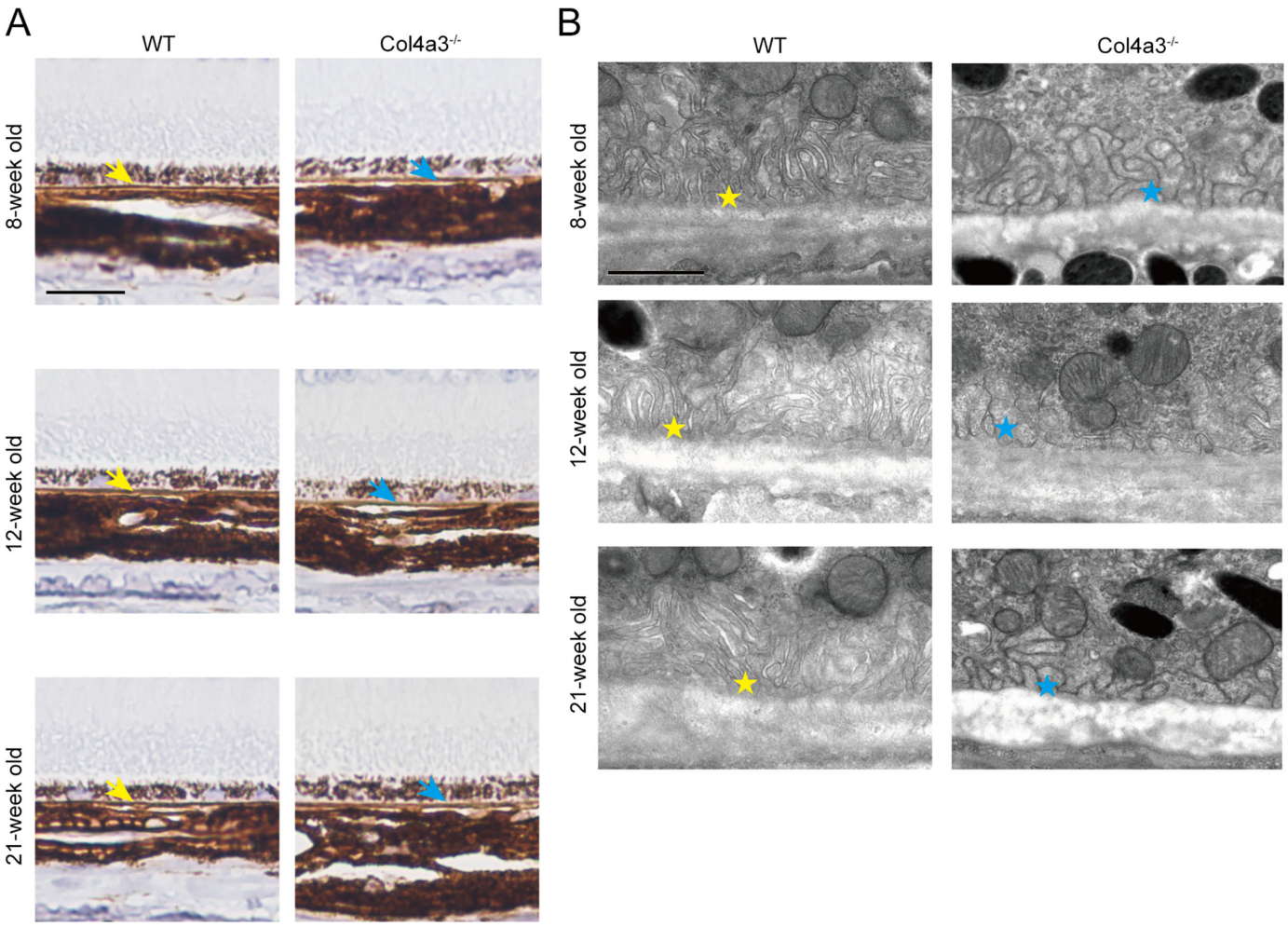

Figure 5. Abnormal membranous structure of the basement membrane of the retinal pigment epithelium in Col4a3$^{-/-}$ mice. (**A**) Collagen IV expression was detected in the basement membrane of the retinal pigment epithelium of Col4a3$^{-/-}$ mice (*blue arrows*) and WT mice (*yellow arrows*). Bar = 20 µm. (**B**) Strip-like basal folds of the retinal pigment epithelium basement membrane were observed under TEM in WT mice (*yellow asterisks*), but thicker, shorter and sparser basal folds were observed in Col4a3$^{-/-}$ mice (*blue asterisks*). Bar = 2 µm.

The thickness of IPL, GCL, INL, and ONL at a site 1000 µm away from the ONH was measured, and we found that the IPL of Col4a3$^{-/-}$ mice was significantly thinner than that of WT mice in all age groups (Fig. 6I), although no significant difference was found in GCL (Fig. 6H), INL (Fig. 6J), or ONL (Supplementary Fig. S3) between the knockout and WT groups.

GFAP Expression was Upregulated in the Col4a3$^{-/-}$ Mice

Because the retinal ILM is composed of Müller cell end feet,[16] we investigated alterations in the glial cell marker GFAP in the retinas of knockout mice. In the retinas of the WT mice, GFAP was expressed at low levels and limited to the retinal nerve fiber layer, GCL, and IPL (Fig. 7A, left panel). In contrast, GFAP expression increased significantly (Fig. 7B) in the Col4a3$^{-/-}$ mice (see Fig. 7A, right panel). Long processes of Müller cells could be observed penetrating through the retinal nerve fiber layer, GCL, IPL, inner nuclear layers, outer plexiform layer, and even outer nuclear layer in all age groups of Col4a3$^{-/-}$ mice (see Fig. 7, black arrows).

Discussion

Alport syndrome (AS) is characterized by basement membrane abnormalities, and ocular lesions are important changes in AS. Approximately 20% to 90% of

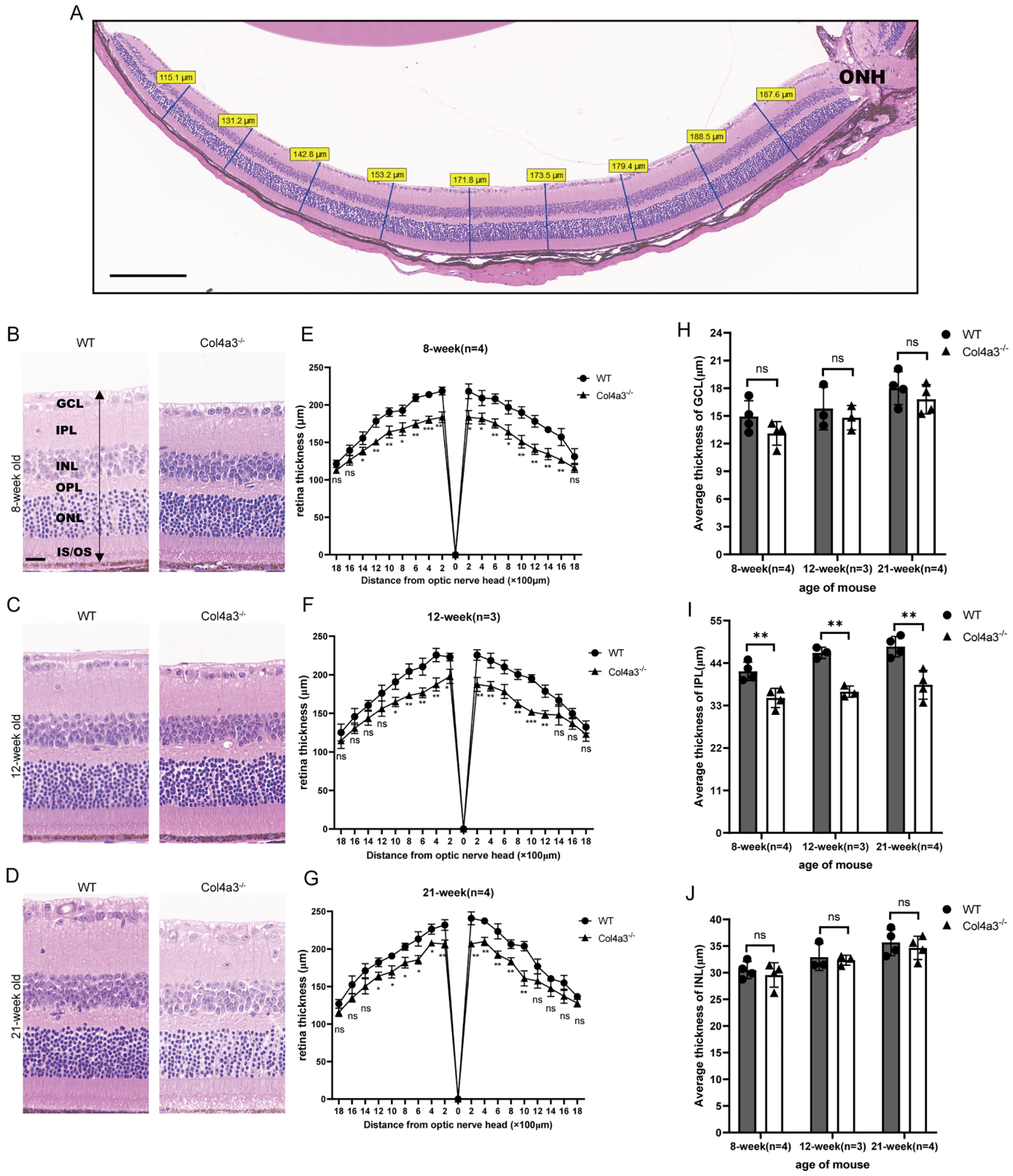

Figure 6. **Retinal thinning in Col4a3$^{-/-}$ mice.** (**A**) Schematic diagram of retinal thickness measurements at nine equidistant positions (indicated with *blue lines*) between ONH and periphery of the retina. Bar = 200 μm. (**B**, **C**, **D**) Representative images of retinas 1000 μm away from the ONH. The range of retinal thickness measured in our study is marked with a *black double-headed arrow* in (**B**). Bar = 20 μm. GCL, ganglion cell layer; IPL, inner plexiform layer; INL, inner nuclear layer; OPL, outer plexiform layer; ONL, outer nuclear layer; IS, inner segment of photoreceptor cells; OS, outer segment of photoreceptor cells. (**E**, **F**, **G**) Qualifications of retinal thickness, (**H**) GCL thickness, (**I**) IPL thickness, →

←

(**J**) INL thickness of all age groups were analyzed on H&E staining images ($n = 3$–4). Data are shown as mean ± SD. ns = P value > 0.05; * = P value < 0.05; ** = P value < 0.01; *** = P value < 0.001.

patients with AS have ocular abnormalities.[1] Some characteristic ocular manifestations, such as anterior lenticonus[17] and temporal retinal thinning,[18] have great value for assisting in the diagnosis of AS. Nevertheless, studies on AS-related ocular diseases are still insufficient. Research on the mechanism of AS ocular disease has been impeded by the lack of an animal model. Although Col4a3$^{-/-}$ mice are widely used to study renal dysfunction induced by AS,[9,10] whether this knockout mouse can serve as a model for AS-associated ocular diseases remains to be explored. With the goal of identifying an animal model to study ocular changes in AS, we characterized the ocular features of Col4a3$^{-/-}$ mice.

Corneal pathological changes in AS, including recurrent corneal epithelial erosion (RCE)[19,20] and posterior corneal pleomorphic atrophy,[21,22] result from abnormalities in the structure of the corneal epithelial basement membrane and Descemet's membrane in the sub-endothelium.[1] A lack of the collagen IV a3a4a5 network in the corneal epithelial basement membrane was found in patients with recurrent corneal epithelial erosion.[19] The research of Hsu et al.[23] showed that abnormalities in collagen IV in the corneal epithelial basement membrane leading to poor adhesion and erosion. Abnormal structure and distribution of the hemidesmosomes of the corneal epithelium are related to reduced epithelial adhesion[12,13] and delayed corneal epithelial wound closure.[24] We found that the expression of collagen IV in the corneal epithelial basement membrane was reduced in Col4a3$^{-/-}$ mice. The ultrastructure of the corneal epithelial basement membrane revealed that the hemidesmosome structure was abnormal in the Col4a3$^{-/-}$ mice. Therefore, we hypothesized that recurrent corneal epithelial erosion in some patients with AS may be due to abnormal hemidesmosomes.

A few reports mentioned posterior corneal pleomorphic atrophy in patients with AS, found vesicular lesions[21] and a network of irregularly arranged hyper-reflective fibrillar structures[22] at the level of Descemet's membrane, but no information was provided on collagen IV changes in Descemet's membrane in patients with AS. In our study, we did not observe differences in collagen IV expression between WT and knockout mice. This indicates that posterior corneal pleomorphic atrophy in patients with AS may not directly result from collagen IV abnormalities.

Lenticonus is a common ocular anomaly of AS that clinically manifests as progressive and aggravated myopia and astigmatism due to abnormal lens shape, mostly involving both eyes. The incidence of lenticonus in patients with AS was reported to be approximately 24% to 37%.[25] Type IV collagen is the most important component of the normal anterior lens capsule,[26] and other components of the lens capsule include type I collagen, type III collagen, laminin, and fibronectin.[27] By electron microscopy, several researchers have found that the anterior lens capsule of patients with AS was thinner than that of healthy people and that there were dehiscences perpendicular to the surface of the capsule located in the inner two-thirds of the anterior lens capsule.[1,17,28] We observed that the anterior lens capsule in Col4a3$^{-/-}$ mice was thinner than that in WT mice in age of the 12-week and the 21-week groups, which was in accordance with previous reports.[28] We noticed abnormally shaped lenses in two 21-week-old Col4a3$^{-/-}$ mice, which resembled the lenticonus observed in patients with AS. Although the shape of the lenticonus in mice is different from that in humans,[29] we presumed that the central protrusion of the lens in Col4a3$^{-/-}$ mice was a result of lens capsule thinning. However, we did not observe splits in the anterior lens capsule of Col4a3$^{-/-}$ mice through TEM analysis, and further investigation is needed to confirm this speculation. The expression of collagen IV in anterior lens capsule did not differ between WT and Col4a3$^{-/-}$ mice because the lens capsule is mainly composed of type IV collagen $\alpha 1$ and $\alpha 2$ chains.[14] Although there was some incongruity in the lens features between knockout mice and patients with AS, which may be due to differences in the composition and structure of collagen IV in the lens capsule between mice and humans, the thinner capsule and abnormal lens shape still make Col4a3$^{-/-}$ mice a potential model for studying the lens abnormities in AS.

Retinopathy in patients with AS mainly manifests as parafoveal fleck retinopathy and temporal retinal thinning. The incidence of fleck retinopathy in patients with AS is about 50% to 70%,[30] whereas the incidence of temporal retinal thinning may be as high as 90% in patients with AS.[4,18] Because mice lack a retinal macular area, we did not study fleck retinopathy in Col4a3$^{-/-}$ mice. Cho et al.[31] examined the retina of patients with AS by stratified Enface optical coherence tomography (OCT) scanning and found retinal flecks in the ILM and RPE basement membrane by horizon-

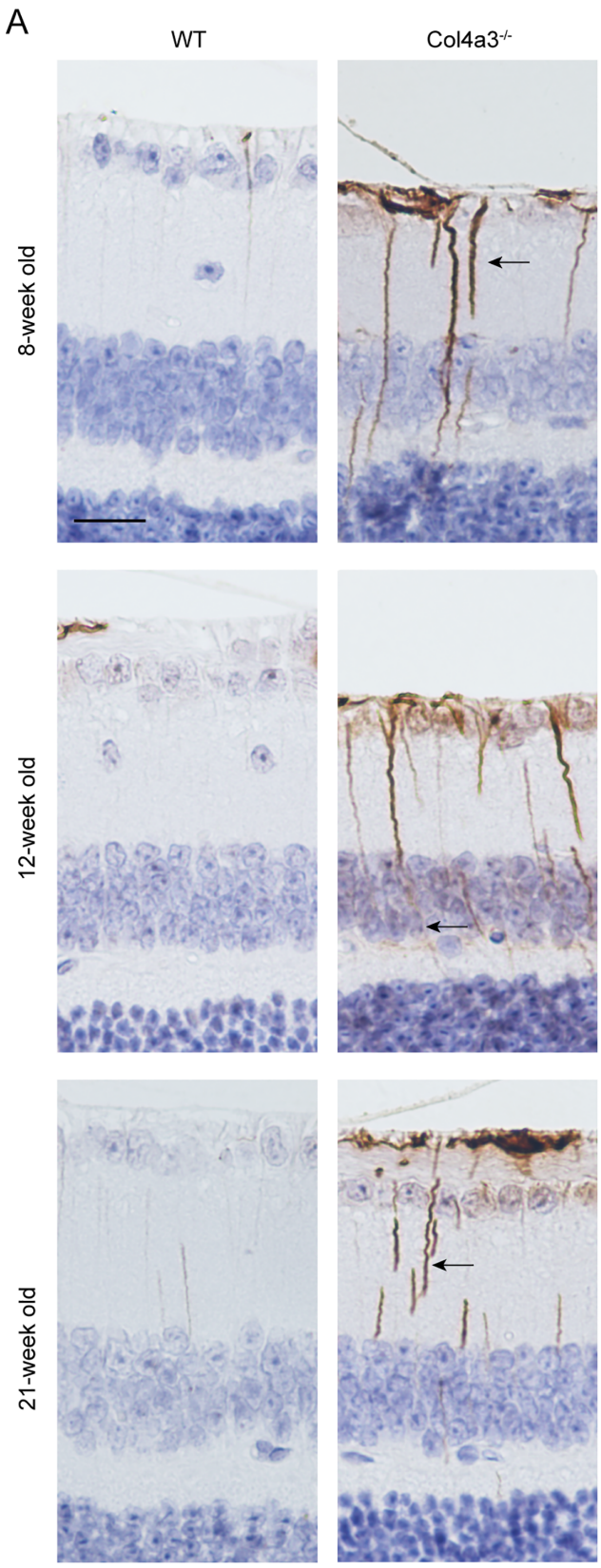

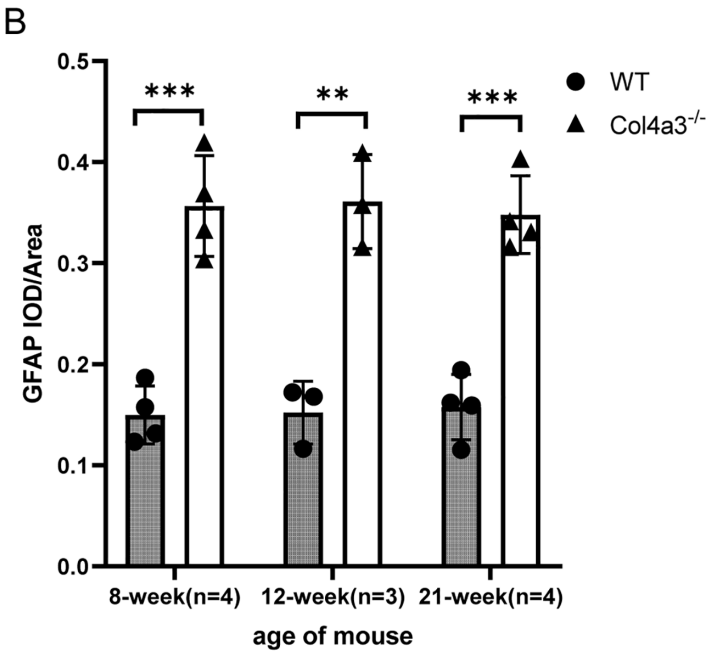

Figure 7. **Increased GFAP level in all age groups of Col4a3$^{-/-}$ mice retina.** (**A**) Immunohistochemistry images showing that GFAP expression was increased in the retinal nerve fiber layer and that GFAP-positive long processes (*black arrows*) penetrated through multiple retinal layers in Col4a3$^{-/-}$ mice. Bar = 20 µm. (**B**) Quantifications of GFAP expression in retina were analyzed on immunohistochemistry images ($n = 3$–4). Data are shown as mean ± SD. ** = P value < 0.01; *** = P value < 0.001.

tal scanning. Savige et al.[32] found that the α3, α4, and α5 chains of type IV collagen were the main components of the ILM and RPE basement membrane. In our study, the expression of collagen IV in the ILM was reduced in Col4a3$^{-/-}$ mice, and the ultrastructure of the ILM was incomplete in Col4a3$^{-/-}$ mice. The ultrastructural changes in the RPE of Col4a3$^{-/-}$ mice revealed that the basal folds of the RPE basement membrane were thicker, shorter, and even absent in certain regions. These findings suggested abnormalities in the ILM and RPE in knockout mice, which could be helpful for elucidating the pathogenesis of retinal flecks.

Temporal retinal thinning is a prominent sign associated with AS. Ahmed et al.[4] reported that in patients with X-linked Alport syndrome (XLAS), 70% had severe thinning and 11% had moderate thinning. Our previous study revealed that 76.74% of patients with XLAS exhibited temporal retinal thinning.[18] Chen et al.[33] reported that 89% of male patients with XLAS, 75% of female patients with XLAS, and 100% of patients with autosomal recessive AS experienced temporal retinal thinning. Researchers have noted that the temporal thinning index (TTI) calculated with retinal thickness is of great value in the diagnosis of AS.[4,33] The pathological basis for temporal retinal thinning has not been elucidated in previous reports. Therefore, an animal model for studying retinal changes will be helpful for exploring the underlying mechanisms involved. We measured the retinal thickness of Col4a3$^{-/-}$ mice, and our results confirmed retinal thinning in knockout mice in all age groups. We previously found that the retinal inner layers were thinning in patients with XLAS, including GCL, IPL, and INL.[18] Furthermore, Savige et al.[32] compared retinal thickness in each quadrant of the macular area in patients with AS and found that the decrease in retinal thickness was due to thinning of the inner layers, including ILM/nerve fiber layer (NFL) and INL. In this study, we found that retinal thinning in Col4a3$^{-/-}$ mice due to the thinning of the IPL, which is in accordance with the results reported in patients. There was no significant difference of ONL thickness between the two groups. ONL is composed of the nuclei of photoreceptors, and it may undergo thinning in cases of vision impairment.[11,34,35] The stable thickness of the ONL may provide an explanation for the preservation of normal vision in the majority of individuals with AS retinal abnormalities.[1] Savige et al.[32] reported that retinopathy of AS may originate in Müller cells. Ahmed et al.[4] speculated that temporal thinning may be related to aberrant Müller cell adhesion. We found that glial cells in knockout mouse retinas were markedly activated, thus further suggesting that Müller cells are involved in retinopathy of AS. The ILM is thinner and more susceptible to tractional forces from the vitreous, which can interfere with nutrient transport and waste clearance in Col4a3$^{-/-}$ mice.[4,32] We also observed an abnormal ILM structure in Col4a3$^{-/-}$ mice. Therefore, we speculate that damage to the ILM caused by abnormal collagen chains leads to an aberrant retinal microenvironment and triggers Müller cell activation. In addition, damaged RPE[31,32,36] and drusen[32,37] detected in patients with AS may result in overlying photoreceptor degeneration and Müller glial cell activation.[38,39] Additionally, we observed abnormalities in the RPE basement membrane under electron microscopy. Consequently, we believe that the upregulation of GFAP in Col4a3$^{-/-}$ mice may be a secondary phenotypic outcome that warrants further investigation.

One of the limitations of our study was that we did not test visual function changes in the knockout mice. Although studies on visual function changes in patients with AS have shown no definite decline in visual sensitivity related to retinal thinning,[1,40] further research on visual function in an AS model is needed. In addition, because of the small number of mice subjected to TEM analysis, more detailed ultrastructural characteristics awaited further investigation. On the other hand, sex differences in the cardiorespiratory phenotype but not in the renal phenotype of C57BL/6 Col4a3$^{-/-}$ mice have been previously reported.[41] Interestingly, there was no sex difference in the ocular phenotype of C57BL/6 Col4a3$^{-/-}$ mice in our study. However, additional studies with larger sample sizes are needed. The impact of sex on different organs of C57BL/6 Col4a3$^{-/-}$ mice might vary greatly. Although previous studies did not document any pathological changes in heterozygous Col4a3$^{+/-}$ mice,[9,42] a 3-year-long study revealed that heterozygous Col4a3$^{+/-}$ mice exhibited renal phenotypes of thin basement membrane nephropathy.[43] This discrepancy may be due to differences in the ages of the Col4a3$^{+/-}$ mice in these investigations. We speculate that heterozygous Col4a3$^{+/-}$ mice might also exhibit ocular manifestations of AS after developing a thin glomerular basement membrane at 30 weeks of age.[43] In this study, we used homozygous Col4a3$^{-/-}$ mice instead of heterozygous mice. However, further investigations are needed to explore the ocular phenotype of Col4a3$^{+/-}$ mice.

In conclusion, for the first time, we described the ocular features of an AS mouse model. Our results provided evidence that Col4a3$^{-/-}$ mice manifested corneal, anterior lens capsule, and retinal anomalies that were consistent with the changes in patients with AS. Col4a3$^{-/-}$ mice could be used as a valuable animal

model to study ocular lesions in AS and other ocular diseases related to the basement membrane, such as RCE, lens capsule anomalies, and ILM disorders. Further explorations are expected to examine the in-depth pathogenesis of the disease.

Acknowledgments

Supported by the National Natural Science Foundation of China (82171059 and 82371064).

Authors' Contributions: Y.W. and R.Z. provided the research design, experiment conduction, data acquisition and analysis, drafting, and critical revision of the manuscript. L.Z. provided the research design and experiment conduction. F.W. and Y.Z. provided the research design and data analysis. S.L. provided the research design and revision of the manuscript. J.D. provided the research design and revision of the manuscript. L.Y. provided the research design, data interpretation, critical revision of the manuscript, and final approval of the version to be published. All authors read and approved the final manuscript.

Disclosure: **Y. Wang**, None; **R. Zhu**, None; **L. Zhao**, None; **F. Wang**, None; **Y. Zhang**, None; **S. Liu**, Sanofi (E, I); **J. Ding**, None; **L. Yang**, None

* YW and RZ contributed equally to this work and share first authorship.

References

1. Savige J, Sheth S, Leys A, et al. Ocular features in Alport syndrome: pathogenesis and clinical significance. *Clin J Am Soc Nephrol*. 2015;10(4):703–709.
2. Nozu K, Nakanishi K, Abe Y, et al. A review of clinical characteristics and genetic backgrounds in Alport syndrome. *Clin Exp Nephrol*. 2019;23(2):158–168.
3. Kashtan CE. Alport Syndrome: achieving early diagnosis and treatment. *Am J Kidney Dis*. 2021;77(2):272–279.
4. Ahmed F, Kamae KK, Jones DJ, et al. Temporal macular thinning associated with X-linked Alport syndrome. *JAMA Ophthalmol*. 2013;131(6):777–782.
5. Herwig MC, Eter N, Holz FG, Loeffler KU. Corneal clouding in Alport syndrome. *Cornea*. 2011;30(3):367–370.
6. Ramakrishnan R, Shenoy A, Meyer D. Ocular manifestations and potential treatments of Alport syndrome: a systematic review. *J Ophthalmol*. 2022;2022:9250367.
7. Savige J. Heterozygous pathogenic COL4A3 and COL4A4 variants (autosomal dominant Alport syndrome) are common, and not typically associated with end-stage kidney failure, hearing loss, or ocular abnormalities. *Kidney Int Rep*. 2022;7(9):1933–1938.
8. Bari A, Mahmood A. Insight into Alport syndrome through ocular imaging. *Asia Pac J Ophthalmol (Phila)*. 2023;12(6):627–628.
9. Cosgrove D, Meehan DT, Grunkemeyer JA, et al. Collagen COL4A3 knockout: a mouse model for autosomal Alport syndrome. *Genes Dev*. 1996;10(23):2981–2992.
10. Guo J, Song W, Boulanger J, et al. Dysregulated expression of microRNA-21 and disease-related genes in human patients and in a mouse model of Alport syndrome. *Hum Gene Ther*. 2019;30(7):865–881.
11. Gao X, Zhu R, Du J, et al. Inhibition of LOX-1 prevents inflammation and photoreceptor cell death in retinal degeneration. *Int Immunopharmacol*. 2020;80:106190.
12. Madigan MC, Holden BA. Reduced epithelial adhesion after extended contact lens wear correlates with reduced hemidesmosome density in cat cornea. *Invest Ophthalmol Vis Sci*. 1992;33(2):314–323.
13. Shams NB, Hanninen LA, Chaves HV, et al. Effect of vitamin A deficiency on the adhesion of rat corneal epithelium and the basement membrane complex. *Invest Ophthalmol Vis Sci*. 1993;34(9):2646–2654.
14. Kalluri R, Cosgrove D. Assembly of type IV collagen. Insights from alpha3(IV) collagen-deficient mice. *J Biol Chem*. 2000;275(17):12719–12724.
15. Kelley PB, Sado Y, Duncan MK. Collagen IV in the developing lens capsule. *Matrix Biol*. 2002;21(5):415–423.
16. Taylor L, Arnér K, Taylor IH, Ghosh F. Feet on the ground: physical support of the inner retina is a strong determinant for cell survival and structural preservation in vitro. *Invest Ophthalmol Vis Sci*. 2014;55(4):2200–2213.
17. Choi J, Na K, Bae S, Roh G. Anterior lens capsule abnormalities in Alport syndrome. *Korean J Ophthalmol*. 2005;19(1):84–89.
18. Zhu RL, Zhao L, Gu XP, et al. Temporal retinal thinning might be an early diagnostic indicator in male pediatric X-linked Alport syndrome. *Int J Ophthalmol*. 2022;15(7):1142–1148.

19. Rhys C, Snyers B, Pirson Y. Recurrent corneal erosion associated with Alport's syndrome. Rapid communication. *Kidney Int*. 1997;52(1):208–211.
20. Burke JP, Clearkin LG, Talbot JF. Recurrent corneal epithelial erosions in Alport's syndrome. *Acta Ophthalmol (Copenh)*. 1991;69(4):555–557.
21. Teekhasaenee C, Nimmanit S, Wutthiphan S, et al. Posterior polymorphous dystrophy and Alport syndrome. *Ophthalmology*. 1991;98(8):1207–1215.
22. Bower KS, Edwards JD, Wagner ME, Ward TP, Hidayat A. Novel corneal phenotype in a patient with Alport syndrome. *Cornea*. 2009;28(5):599–606.
23. Hsu JK, Rubinfeld RS, Barry P, Jester JV. Anterior stromal puncture. Immunohistochemical studies in human corneas. *Arch Ophthalmol*. 1993;111(8):1057–1063.
24. Kim EC, Kim DJ, Lee SS, Kim MS. Ultrastructural changes of cornea after ethanol ingestion in Otsuka Long-Evans Tokushima fatty (OLETF) and Long-Evans Tokushima Otsuka (LETO) rats. *Graefes Arch Clin Exp Ophthalmol*. 2010;248(10):1457–1466.
25. Colville DJ, Savige J. Alport syndrome. A review of the ocular manifestations. *Ophthalmic Genet*. 1997;18(4):161–173.
26. Cummings CF, Hudson BG. Lens capsule as a model to study type IV collagen. *Connect Tissue Res*. 2014;55(1):8–12.
27. Halfter W, Moes S, Halfter K, et al. The human Descemet's membrane and lens capsule: protein composition and biomechanical properties. *Exp Eye Res*. 2020;201:108326.
28. Streeten BW, Robinson MR, Wallace R, Jones DB. Lens capsule abnormalities in Alport's syndrome. *Arch Ophthalmol*. 1987;105(12):1693–1697.
29. Chakraborty R, Lacy KD, Tan CC, Park HN, Pardue MT. Refractive index measurement of the mouse crystalline lens using optical coherence tomography. *Exp Eye Res*. 2014;125:62–70.
30. Liu J, Colville D, Wang YY, et al. The dot-and-fleck retinopathy of X linked Alport syndrome is independent of complement factor H (CFH) gene polymorphisms. *Br J Ophthalmol*. 2009;93(3):379–382.
31. Cho IH, Kim HD, Jung SJ, Park TK. En face optical coherence tomography findings in a case of Alport syndrome. *Indian J Ophthalmol*. 2017;65(9):877–879.
32. Savige J, Liu J, DeBuc DC, et al. Retinal basement membrane abnormalities and the retinopathy of Alport syndrome. *Invest Ophthalmol Vis Sci*. 2010;51(3):1621–1627.
33. Chen Y, Colville D, Ierino F, Symons A, Savige J. Temporal retinal thinning and the diagnosis of Alport syndrome and thin basement membrane nephropathy. *Ophthalmic Genet*. 2018;39(2):208–214.
34. Ersoz MG, Karacorlu M, Arf S, Hocaoglu M, Sayman Muslubas I. Outer nuclear layer thinning in pachychoroid pigment epitheliopathy. *Retina*. 2018;38(5):957–961.
35. Oishi A, Fang PP, Thiele S, Holz FG, Krohne TU. Longitudinal change of outer nuclear layer after retinal pigment epithelial tear secondary to age-related macular degeneration. *Retina*. 2018;38(7):1331–1337.
36. Savige J, Wang Y, Crawford A, et al. Bull's eye and pigment maculopathy are further retinal manifestations of an abnormal Bruch's membrane in Alport syndrome. *Ophthalmic Genet*. 2017;38(3):238–244.
37. Friedburg D. Pseudoneuritis and drusen of the optic disk in Alport's syndrome. *Klin Monbl Augenheilkd*. 1968;152(3):379–383.
38. Johnson PT, Lewis GP, Talaga KC, et al. Drusen-associated degeneration in the retina. *Invest Ophthalmol Vis Sci*. 2003;44(10):4481–4488.
39. Kovács-Valasek A, Rák T, Pöstyéni E, Csutak A, Gábriel R. Three major causes of metabolic retinal degenerations and three ways to avoid them. *Int J Mol Sci*. 2023;24(10):8728.
40. Wong EN, Tay-Kearney ML, Chen FK. Structure-function correlation of focal and diffuse temporal perifoveolar thinning in Alport syndrome. *Clin Exp Ophthalmol*. 2014;42(7):699–702.
41. Irion CI, Williams M, Capcha JC, et al. Col4a3$^{-/-}$ mice on Balb/C background have less severe cardiorespiratory phenotype and SGLT2 overexpression compared to 129x1/SvJ and C57Bl/6 backgrounds. *Int J Mol Sci*. 2022;23(12):6674.
42. Miner JH, Sanes JR. Molecular and functional defects in kidneys of mice lacking collagen alpha 3(IV): implications for Alport syndrome. *J Cell Biol*. 1996;135(5):1403–1413.
43. Beirowski B, Weber M, Gross O. Chronic renal failure and shortened lifespan in COL4A3+/− mice: an animal model for thin basement membrane nephropathy. *J Am Soc Nephrol*. 2006;17(7):1986–1994.